Flow-induced vibration of a circular cylinder subjected to wake interference at low Reynolds number

B.S. Carmo [a,*], S.J. Sherwin [a], P.W. Bearman [a], R.H.J. Willden [b]

[a] *Department of Aeronautics, Imperial College London, UK*

[b] *Department of Engineering Science, University of Oxford, UK*

Received ??; received in revised form ??; accepted ??

Abstract

Two- and three-dimensional numerical simulations of the flow around two circular cylinders in tandem arrangements are performed. The upstream cylinder is fixed and the downstream cylinder is free to oscillate in the transverse direction, in response to the fluid loads. The Reynolds number is kept constant at 150 for the two-dimensional simulations and at 300 for the three-dimensional simulations, and the reduced velocity is varied by changing the structural stiffness. The in-line centre-to-centre distance is varied from 1.5 to 8.0 diameters, and the results are compared to that of a single isolated flexible cylinder with the same structural characteristics, $m^* = 2.0$ and $\zeta = 0.007$. The calculations show that significant changes occur in the dynamic behaviour of the cylinders, when comparing the flow around the tandem arrangements to that around an isolated cylinder: for the tandem arrangements, the lock-in boundaries are wider, the maximum displacement amplitudes are greater and the amplitudes of vibration for high reduced velocities, outside the lock-in, are very significant. The main responsible for these changes appears to be the oscillatory flow in the gap between the cylinders.

Keywords: Flow-induced vibration; circular cylinder; wake interference

* Corresponding author. Current address: NDF, POLI, University of São Paulo, Brazil

Tel.: +55 11 3091 9636; fax: +55 11 3091 5642.

E-mail address: bruno.carmo@usp.br (B.S. Carmo).

1. Introduction

The flow around circular cylinders has been extensively studied due to its practical importance in engineering and scientific relevance in fluid mechanics. On the engineering side, there are a number of devices in mechanical, civil and naval engineering where circular-cylindrical structures are used. Examples of such devices are heat exchangers, chimneys and offshore platforms. In scientific terms, the flow around circular cylinders exhibits various important physical phenomena, such as separation, vortex shedding and turbulence in the wake, at relatively low Reynolds numbers.

When circular cylinders are grouped in close proximity, the flow field and the forces experienced by the cylinders can be entirely different from those observed when the bodies are isolated in the fluid stream. The effect of the presence of other bodies in the flow is called *flow interference*, and it has crucial importance in aerodynamics and hydrodynamics. For example, in all the devices mentioned in the previous paragraph it is common to have circular-cylindrical structures grouped together. One of the most severe types of interference, and the type on which this paper focuses, is *wake interference*, which happens when the cylinder is immersed or in close proximity to the wake of another bluff body. In such situations, the flow impinging on the cylinder is usually totally different from the free stream. Given the number of differences observed in the forces exerted on cylinders subjected to wake interference when compared to the single cylinder case, one expects that the flow-induced vibrations (FIV) experienced by a flexible cylinder or a compliantly-mounted rigid cylinder will also be different depending whether the cylinder is immersed in a vortex wake or not. A few papers on this matter have been published, most of them were concerned with vibrations within the synchronisation range, i.e. when the vortex shedding is synchronised with the cylinder vibration.

Scientific works on FIV of bluff bodies subjected to wake interference started to appear around three decades ago, and experimental papers on the subject have been consistently published since then. King and Johns (1976) investigated the vibration of two flexible cylinders in tandem by performing experiments in a water channel. Bokaian and Geoola (1984) carried out experiments on the flow around circular cylinders in tandem and staggered arrangements, the upstream cylinder being fixed and the downstream one being rigid and mounted on an elastic base that allowed cross-stream displacement. Zdravkovich (1985) investigated the behaviour of two flexible circular cylinders placed in diverse arrangements using a wind tunnel. Brika and Laneville (1999) utilised wind tunnel experiments to study the flow induced vibrations of a flexible circular cylinder, allowed to vibrate in one plane only, immersed in the wake of a rigid cylinder. Assi et al. (2006) performed experiments on the FIV of a elastically-mounted rigid cylinder in the wake of a fixed identical cylinder, using a water channel. Recently, there has also been a few computational studies on FIV of two circular cylinders in tandem. Examples of this type of work are Mittal and Kumar (2001), Jester and Kallinderis (2004) and Papaioannou et al. (2008). In all these papers, the

computations were two-dimensional and focused on reduced velocities within the synchronisation range. In general terms, they confirmed the main conclusions of previously published experimental data: the wake interference led to a wider synchronisation range and within this range the amplitude of response was larger than that observed in the response of an isolated cylinder with the same structural parameters.

However, some papers have also reported that cylinders subjected to wake interference also experienced vibrations with high amplitudes for higher reduced velocities, outside the synchronisation range (Bokaian and Geoola, 1984; Zdravkovich, 1985; Brika and Laneville, 1999; Hover and Triantafyllou, 2001). In most cases, the amplitude levels were even higher than those observed in the lock-in. Although the reduced velocity for which this peculiar type of response starts to be significant seems to depend on various aspects, such as the separation between the cylinders and the mass ratio, all the papers agree on the fact that an upper reduced velocity limit for which these vibrations would cease does not seem to exist. There has not been a consensus on the physical mechanism of this response, and this is reflected in the myriad of different names used to refer to it: wake-induced galloping (Bokaian and Geoola, 1984), fluid-elastic response (Zdravkovich, 1985), wake interference galloping (Brika and Laneville, 1999) and galloping (Hover and Triantafyllou, 2001) are some examples.

As we can see, the number of publications on flows around circular cylinders affected by wakes of other circular cylinders is not small. However, the parameter space to be investigated in such flows is considerably larger than in the flow around an isolated cylinder. For instance, we can vary the streamwise and cross-stream separations between the bodies, the orientation of the axis of the cylinders, the number of cylinders and the ratio between the diameters of the cylinders. Furthermore, in the case of FIV, we can also consider some cylinders fixed and others allowed to oscillate in one or two directions, in addition to using different structural parameters for each cylinder. Because of this large number of parameters to be analysed, the basic understanding about flows with wake interference is far from being comparable to the knowledge on the flow around an isolated cylinder. This paper aims at decreasing this gap.

A complementary approach to tackling problems with such a large parameter space is to model the phenomenon based on a deep understanding of its physics, obtained by the investigation of one or a few simple cases where the phenomenon is present. If the model is sufficiently consistent with the physics, its extrapolation to a number of other similar cases is likely to be valid. Therefore, to understand how the approaching wake interacts with a compliant body, we investigated the flow around a circular cylinder mounted on an elastic basis, allowed to move only in the transverse direction, immersed in the wake of an upstream fixed circular cylinder of the same diameter D placed at a streamwise centre-to-centre distance L_x, as sketched in figure 1. This is a very useful model to study wake interference, since the number of parameters is kept to a reasonable quantity for a proper systematic analysis so the basics of the interference mechanisms can be more easily understood. Although we also present results for reduced velocities in the synchronisation range, we focus particularly on the high reduced

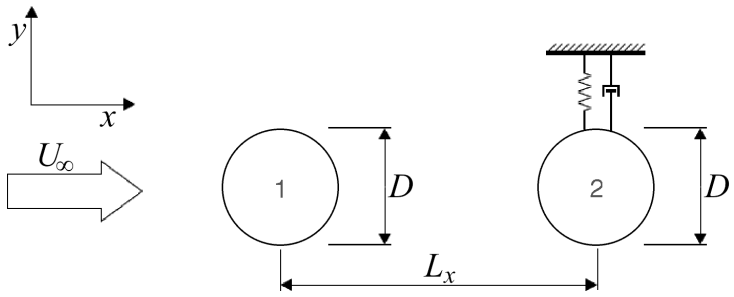

Fig. 1. Schematic drawing of arrangement studied.

velocity response of the downstream cylinder. Two- and three-dimensional numerical simulations were employed to get physical insight into the mechanism responsible for the high amplitudes of vibration that are observed. The main goal of this investigation is to consider the FIV of the downstream cylinder in tandem arrangements, so as to clarify the physical mechanisms involved.

The remainder of this paper is organised as follows: in section 2. the methodology employed to study the phenomenon is outlined. In section 3. the results of the two- and three-dimensional simulations of the flow around a single cylinder and around two cylinders in different tandem arrangements are presented and analysed. In section 4. we discuss the applicability of two- and three-dimensional simulations, the physical mechanism responsible for the cylinder vibration and a comparison between the current results and previously published experimental data. Finally, in section 5. conclusions and recommendations for future work are drawn.

2. Numerical method for the flow-induced vibration simulations

In this section, the numerical tools employed to study the FIV of a compliantly-mounted circular cylinder immersed in the wake of an identical fixed body are described. We delineate the mathematical model of the structure, outline the mathematical framework used to include the domain deformation into the flow equations and explain how the flow-structure coupling was incorporated into the time discretisation scheme.

2.1. Flow equations

The flows investigated in this paper were calculated using numerical simulations of the incompressible Navier–Stokes equations, here written in non-dimensional form:

$$\frac{\partial \mathbf{u}}{\partial t} = -(\mathbf{u}.\nabla)\mathbf{u} - \nabla p + \frac{1}{Re}\nabla^2\mathbf{u}, \tag{1}$$

$$\nabla.\mathbf{u} = 0. \tag{2}$$

The cylinder diameter D is the reference length and the free-stream speed U_∞ is the reference speed used in the non-dimensionalisation. $\mathbf{u} \equiv (u, v, w)$ is the velocity field, t is the time, p is the modified static pressure, i.e.

divided by the constant density ρ, $Re = \rho U_\infty D/\mu$ is the Reynolds number and μ is the dynamic viscosity of the fluid. The numerical solution of these equations was calculated using a Spectral/hp discretisation as described in Karniadakis and Sherwin (2005).

2.2. Structure equation

In the FIV problems considered in this paper, we assumed that the moving cylinder was rigid and mounted on an elastic base that allows displacement in only one direction; such behaviour of an oscillating structure is described by the equation of a linear mass-spring-damper system forced by the fluid load. This equation can be written in non-dimensional form as

$$M^* \ddot{y}_c^* + C^* \dot{y}_c^* + K^* y_c^* = F_y^*(\ddot{y}_c^*, \dot{y}_c^*, y_c^*, t^*), \tag{3}$$

where M^* is the non-dimensional mass of the oscillating system, C^* is the non-dimensional structural damping coefficient, K^* the non-dimensional stiffness coefficient and F_y^* is the non-dimensional force imposed by the fluid in the direction of motion. These non-dimensional parameters are related to their dimensional counterparts M, C, K and F_y by the expressions

$$M^* = \frac{M}{\rho D^2 L}, \qquad C^* = \frac{C}{\rho U_\infty D L}, \qquad K^* = \frac{K}{\rho U_\infty^2 L}, \qquad F_y^* = \frac{C_L}{2} = \frac{F_y}{\rho U_\infty^2 D L},$$

where L is the (axial) length of the cylinder and C_L is the lift coefficient. The variables $\ddot{y}_c^*$, $\dot{y}_c^*$, y_c^* are the non-dimensional acceleration, velocity and displacement of the body, respectively, and t^* is the non-dimensional time. These variables are non-dimensionalised according to the expressions

$$\ddot{y}_c^* = \frac{\ddot{y}_c D}{U_\infty^2}, \qquad \dot{y}_c^* = \frac{\dot{y}_c}{U_\infty}, \qquad y_c^* = \frac{y_c}{D}, \qquad t^* = \frac{t U_\infty}{D}.$$

This non-dimensionalisation scheme was adopted in order to make the non-dimensional form of the structure and flow equations consistent, so the coupling between the structure and flow solvers could be more easily undertaken. However, M^*, C^* and K^* are not the most common choice of non-dimensional parameters in the literature. For ease of comparison with previously published data, the results of this paper are presented as a function of the mass ratio, m^*, damping ratio, ζ, and reduced velocity, V_r. These non-dimensional parameters are defined as

$$m^* \equiv \frac{4M}{\rho \pi D^2 L}, \qquad \zeta \equiv \frac{C}{2\sqrt{KM}}, \qquad V_r \equiv \frac{U_\infty}{f_n D}.$$

where f_n is the natural frequency of the structure in a vacuum ($f_n = \sqrt{K/M}/(2\pi)$). The non-dimensional parameters of the structural equation (3) are related to m^*, ζ and V_r by the expressions

$$M^* = \frac{\pi m^*}{4}, \qquad C^* = \frac{\pi^2 m^* \zeta}{V_r}, \qquad K^* = \frac{\pi^3 m^*}{V_r^2}.$$

2.3. Arbitrary Lagrangian-Eulerian formulation

The fluid-structure interaction problem this paper of interest comprises the flow around two bodies, with one of them being allowed to move independently of the other. The computational code used to simulate the flow therefore uses an Arbitrary Lagrangian-Eulerian (ALE) formulation was employed. The ALE formulation allows one to incorporate arbitrary displacements of the mesh into the governing equations, so the movement of the bodies and the mesh deformations necessary to maintain an adequate spatial discretisation can be taken into account.

The ALE incompressible Navier-Stokes equations (1)–(2) involve a simple modification in the advection term:

$$\frac{\partial \mathbf{u}}{\partial t} = -(\mathbf{u} - \mathbf{m}) \cdot \nabla \mathbf{u} - \nabla p + \frac{1}{Re} \nabla^2 \mathbf{u}, \tag{4}$$

$$\nabla \cdot \mathbf{u} = 0, \tag{5}$$

where $\mathbf{m}$ is the velocity of the coordinate systems attached to the mesh, also referred to as velocity of the mesh. The pressure and viscous terms as well as the continuity equation (5) do not need to be altered because they are independent of time, and their dependence on space is not altered by simple translation or divergence of the coordinate systems. Equations (4) and (5) are the Arbitrary Lagrangian-Eulerian form of the Navier-Stokes equations.

2.4. Flow-structure coupling and time discretisation

The equations (3), (4) and (5) have to be solved in a coupled manner. The fluid load F_y^* in eq. (3) is calculated from the solution of the flow equations (4)-(5), and the motion of the boundaries, which are necessary for the solution of eqs. (4)-(5), is determined by the solution of the structure equation (3). The dependency of the fluid force F_y^* on the position, velocity and acceleration of the body makes the coupled problem strongly nonlinear.

The algorithm below describes the time splitting scheme used in the FIV simulations. The structure and flow solvers are loosely coupled, similar to the work of in Jester and Kallinderis (2004), since the time step sizes necessary for the solution of the flow equations (i.e. the CFL restriction) were sufficiently small to yield convergent loosely-coupled schemes. The mesh movement is incorporated to the time splitting scheme in a similar fashion as in Beskok and Warburton (2001). Given a certain state of the flow, mesh and structure variables at time level n $(\mathbf{u}^n, p^n, \mathbf{x}^n, \mathbf{m}^n, y_c^{*n}, \dot{y}_c^{*n})$, these variables are advanced to time level $n+1$ according to the following steps:

(1) Calculate $\mathbf{N}(\mathbf{u}^n, \mathbf{m}^n) = (\mathbf{u}^n - \mathbf{m}^n).\nabla \mathbf{u}^n$

(2) Solve structural equation (find $y_c^{*\,n+1}$ and $\dot{y}_c^{*\,n+1}$)

(3) Calculate $\mathbf{m}^{n+1}$

(4) Calculate the pressure boundary conditions:

$$\frac{\partial \bar{p}^{n+1}}{\partial n} = \mathbf{n} \cdot \left\{ -\frac{\partial \mathbf{u}^{n+1}}{\partial t} + \sum_{q=0}^{J_e-1} \beta_q \left[\mathbf{N}(\mathbf{u}^{n-q}, \mathbf{m}^{n-q}) - \frac{1}{Re}(\nabla \times (\nabla \times \mathbf{u}^{n-q})) \right] \right\} \tag{6}$$

(5) Calculate the new position of the mesh nodes, $\mathbf{x}^{n+1}$

(6) Integrate the advection terms:

$$\check{\mathbf{u}} = \Delta t \sum_{q=0}^{J_e-1} \beta_q \mathbf{N}(\mathbf{u}^{n-q}, \mathbf{m}^{n-q}) + \sum_{q=0}^{J_i-1} \alpha_q \mathbf{u}^{n-q}$$

(7) Set and solve linear system for pressure:

$$\nabla^2 \bar{p}^{n+1} = \nabla \cdot \left(\frac{\check{\mathbf{u}}}{\Delta t} \right) \tag{7}$$

(8) Set and solve linear system for velocity:

$$\nabla^2 \mathbf{u}^{n+1} - \frac{Re\gamma_0}{\Delta t} \mathbf{u}^{n+1} = Re \left(\nabla \bar{p}^{n+1} - \frac{\check{u}}{\Delta t} \right) \tag{8}$$

The coefficients γ_0, α_q and β_q are those from the stiffly-stable scheme presented by Karniadakis et al. (1991).

Steps 1 and 6 deal with the nonlinear advection term of the ALE-Navier-Stokes equations and are fully explicit. In step 2, the structure equation (3) is integrated using Newmark's scheme (Newmark, 1959). The mesh velocity, $\mathbf{m}^{n+1}$, and coordinates, $\mathbf{x}^{n+1}$, are calculated in steps 3 and 5 of the algorithm. In ALE implementations, an automatic mesh deformation procedure is usually employed to perform these calculations. In this work, we used the method proposed by Batina (1990), in which the mesh is adapted to the boundary displacement in every time step by modelling each edge of the mesh as a spring with stiffness inversely proportional to its length. Having the new mesh coordinates $\mathbf{x}^{n+1}$, the mesh velocities were calculated consistently with the stiffly-stable method

$$\mathbf{m}^{n+1} = \frac{\gamma_0 \mathbf{x}^{n+1} - \sum_{q=0}^{J_i-1} \alpha_q \mathbf{x}^{n-q}}{\Delta t}.$$

So, in practice, both $\mathbf{x}^{n+1}$ and $\mathbf{m}^{n+1}$ are calculated in step 3, but the coordinate information is only updated in the flow solver data structures in step 5, after the pressure boundary conditions are calculated.

The term $\partial \mathbf{u}^{n+1}/\partial t$ in eq. (6) is also calculated using an approximation consistent with the stiffly-stable scheme:

$$\frac{\partial \mathbf{u}^{n+1}}{\partial t} = \frac{\gamma_0 \mathbf{u}^{n+1} - \sum_{q=0}^{J_i-1} \alpha_q \mathbf{u}^{n-q}}{\Delta t}.$$

The value of the acceleration is only needed at the boundary, and this is given by the solution of the structural equation.

The method presented above was validated using arbitrary motion of the mesh elements in simple steady flows and verifying that all the flow variables were conserved. We also compared the results obtained for the flow around

a circular cylinder mounted in a elastic base allowed to move in the cross-stream direction with reduced velocity $V_r = 6.0$ and $Re = 100$ using the ALE algorithm and solving the flow equations in the frame of reference attached to the body (Li et al., 2002). The amplitude and frequency of the cylinder response and of the forces on the cylinder obtained in the two tests agreed within a tolerance of 0.1%.

Another aspect of Finite Element discretisations is that, for linear equations such as (7) and (8), the elemental matrices depend only on certain geometric information about the elements. This information is invariant to translation, thus for an element of a given shape and size, the matrix corresponding to a certain linear operator is independent of where this element is located in relation to the absolute frame of reference, as long as the element's orientation does not change. Since the FIV problems that concern this paper comprise purely translational movements, we can take advantage of the translational symmetry of the discretisation by making most of the elements to either rigidly translate with the moving body or to remain steady and not deform, so the number of elemental matrices to be re-generated, and consequently the number of modifications in the global system, is minimised. It is also convenient to deform elements that are away from the bodies, so we assure that the mesh close to the bodies keeps its quality. Figure 2 shows an example of a mesh used in the flow-induced vibration simulations. Notice that all the deformable elements are triangles, and that the regions where the mesh is rigid are defined such that the number of deformable elements is kept to a minimum (for more details on the meshing strategy, see Carmo, 2009).

3. Results

The configurations tested had separations $L_x/D = 1.5$, 3, 5 and 8. These configurations were chosen because of the different shedding regimes they present for fixed arrangements (for a classification of shedding regimes, see for example Zdravkovich, 1987; Carmo et al., 2010). In addition, simulations of the flow around a single cylinder mounted on an elastic base with the same structural parameters were performed, to serve as a benchmark. The meshes employed were variations of that shown in figure 2, keeping the same discretisation strategy. The number of elements varied from 507 to 811 depending on the configuration, and Jacobi polynomials of degree 8 were used in the expansion base. The boundaries of the meshes were located $36D$ upstream from the upstream cylinder, $45D$ downstream from the downstream cylinder and $50D$ from the centres of the cylinders in the cross-stream direction on both sides. For the three-dimensional simulations, a spanwise periodic length of $12D$ discretised with 32 Fourier modes was used. The size of the mesh and level of discretisation were based on the convergence studies in Carmo (2005), in which simulations of flows around the same arrangements in the same Reynolds number range, but with both cylinders fixed were performed. Uniform stream velocity boundary conditions ($u = 1$, $v = 0$) were imposed at the upstream and side boundaries of the computational domain. At the cylinder walls, a no-slip condition was

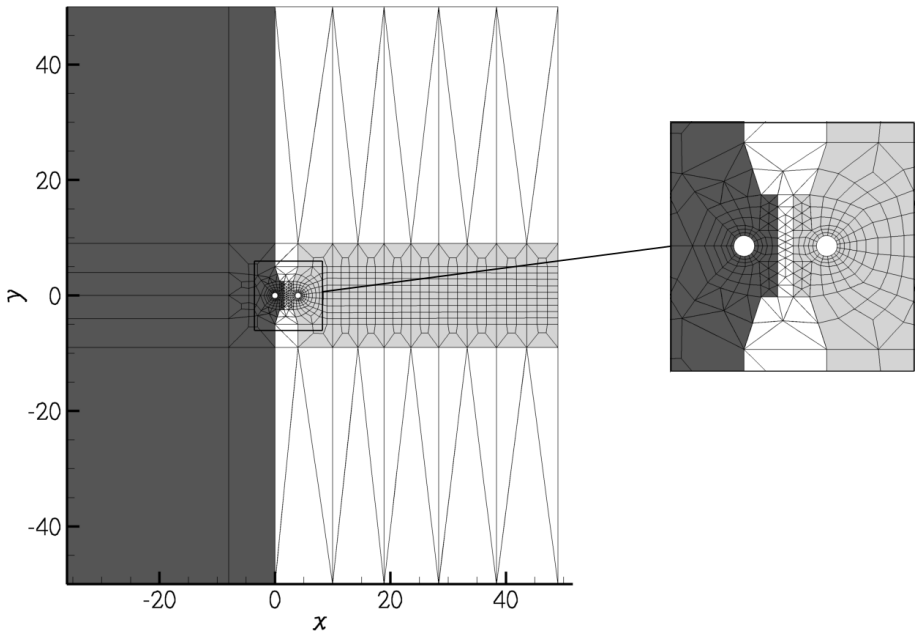

Fig. 2. Example of a mesh used with the ALE formulation, showing also the detail of the discretisation close to the cylinders. The dark grey region remains fixed, the elements in the light grey region move rigidly with the downstream cylinder and the elements in the white region deform to comply with the movement of the cylinder.

imposed so the fluid had the same velocity as the body, and at the downstream boundary Neumann conditions, $\partial u/\partial \mathbf{n}$=0, $\partial v/\partial \mathbf{n} = 0$ were applied. Uniform pressure was imposed at the downstream boundary, and its value was used as the reference pressure for the calculations.The high-order boundary condition given by equation (6) was used on all other boundaries.

The mass ratio and structural damping of the elastic base were $m^* = 2.0$ and $\zeta = 0.007$, chosen to match the structural parameters of the experiments carried out by Assi et al. (2008). The reduced velocities tested ranged from 3.0 to 30.0, varied by changing the spring stiffness and keeping the Reynolds number constant. The Reynolds number was 150 for the two-dimensional simulations and 300 for the three-dimensional simulations. The non-dimensional time steps were 0.006 and 0.003 for the two- and three-dimensional simulations, respectively. All FIV simulations were started from fully-developed flows obtained from two-dimensional simulations with the cylinders fixed and $Re = 150$.

3.1. Two-dimensional simulations

We first present the results from the FIV of an isolated cylinder in section 3.1.1.. Next we discuss the results obtained for configurations with small separations in section 3.1.2., and with large separations in section 3.1.3..

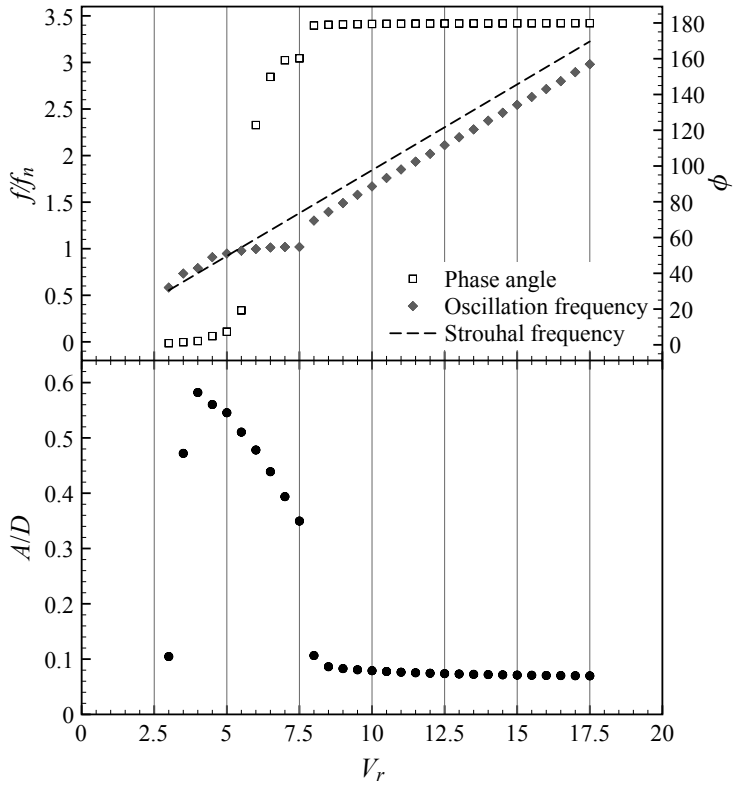

Fig. 3. Non-dimensional amplitude (A/D), phase angle (ϕ) and frequency plots against reduced velocity for the flow around an isolated cylinder, $Re = 150$, two-dimensional simulations. The Strouhal frequency is the vortex shedding frequency in the flow around a fixed cylinder at the same Reynolds number.

3.1.1. Single cylinder

The results obtained for the flow around a single cylinder (figure 3) show the typical response of vortex-induced vibrations at low Reynolds numbers and low mass ratio (see figure 12 in Williamson and Govardhan, 2004). There is a very well defined lock-in range, where the vortex shedding frequency locks to a value close to the natural frequency of the structure, as can be seen in the frequency plot in figure 3. The lock-in range can be divided into an initial and a lower branch. The initial branch covers the range $3.0 \leq V_r \leq 5.5$, and has a phase angle ϕ close to 0°. It is in the initial branch that the amplitude reaches its highest value for the reduced velocities investigated, $A/D = 0.582$. For $5.5 < V_r < 6.0$ the phase angle changes abruptly from a value close to 0° to a value close to 180°, and this marks the transition between the initial and lower branches. The lower branch extends from $V_r \approx 6.0$ to $V_r \approx 7.5$, and for this range the cylinder exhibits fairly large amplitudes of vibration ($0.3 < A/D < 0.5$). For reduced velocities higher than those of the lower branch ($V_r \geq 8.0$) the amplitude of vibration is low ($A/D < 0.1$), and the phase angle is close to 180°.

3.1.2. Tandem arrangements – small separations

The structural responses in the two-dimensional simulations for the configurations $L_x/D = 1.5$ and $L_x/D = 3.0$ were very similar; figure 4 shows the results for $L_x/D = 3.0$. The synchronisation range starts at $V_r \approx 4.0$; this reduced velocity is higher than that for which the synchronisation range starts for the single cylinder ($V_r \approx 3.0$, see figure 3). This can be explained by the fact that the mean flow in the wake is slower than the free stream. Like the isolated cylinder, the lock-in region for the tandem arrangements with small separations can be divided into an initial and a lower branch. The initial branch covers $4.0 \leq V_r \leq 6.0$, and exhibits the highest amplitudes of the entire response range. The peak amplitude was observed for $V_r = 6.0$ and its value was slightly higher than $0.9D$, which is more than 50% larger than the peak amplitude observed for the isolated cylinder. As the reduced velocity is increased, the initial branch is followed by a lower branch, where the amplitude of vibration decreases smoothly, instead of showing the abrupt decrease observed for the single cylinder case. For the tandem arrangements, the range for which the downstream cylinder vibrates with significant amplitudes does not have an upper V_r limit like in the single cylinder case. For reduced velocities from 15 up to 30, the amplitude of vibration is surprisingly high (between $0.4D$ and $0.5D$), and the phase angle is close to 180°. In this same velocity range, the isolated cylinder vibrated with negligible amplitudes ($A/D < 0.1$).

Regarding the frequency of vibration, also shown in figure 4, it can be seen that for the first few points the frequencies follow the Strouhal line, but they stop coinciding as soon as the amplitude of vibration becomes large. For $4.5 \leq V_r \leq 8.0$, the frequency of vibration is close to the natural frequency of the structure, but the data points show an almost parallel trend to the Strouhal frequency, different from the flat plateau observed for the single cylinder case in the lock-in region. It is also in this reduced velocity range, more specifically for $6.0 < V_r < 6.5$, that the phase angle jump occurs. For $V_r > 8.5$ the frequency of vibration follows a linear trend with positive slope; however this slope is different from that of the Strouhal line for the fixed arrangement. The reason for this can be identified by looking at the vorticity contours in figure 5. Once the downstream cylinder starts to vibrate with a reasonable amplitude, the shedding regime changes from that of when the cylinder is fixed, and so does the main frequency of shedding and consequently the frequency of oscillation.

It should be noted that when the downstream cylinder is vibrating with high amplitudes, the vortices roll up upstream of the leeward cylinder, but they are still connected to the upstream cylinder through the shear layer when they impinge on the downstream cylinder. The complete detachment of the vortex from the upstream body happens only as the downstream cylinder moves across the wake, cutting off the shear layer, as illustrated by the sequence of three contour plots in figure 6. Consequently, for configurations with small separations the motion of the downstream cylinder is tightly coupled with the vortex shedding from the upstream cylinder. The normalised power spectral density (PSD) contours of the displacement and upstream lift coefficient signals shown in figure 7 show that the spectra of these signals are practically the same. An important conclusion from this observation is

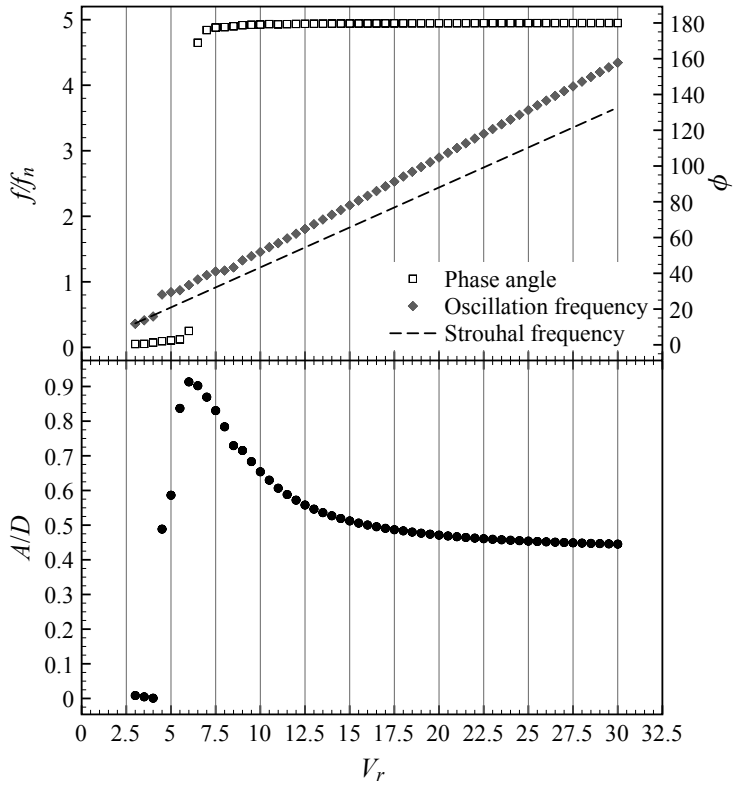

Fig. 4. Amplitude, phase angle and frequency plots against reduced velocity for the downstream cylinder in a tandem arrangement with $L_x/D = 3$, $Re = 150$, two-dimensional simulations.

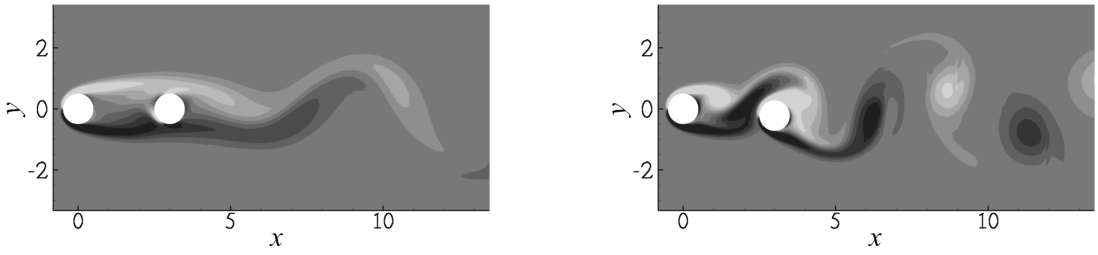

(a) Fixed cylinders (b) $V_r = 10.0$

Fig. 5. Instantaneous vorticity contours illustrating different shedding regimes. $L_x/D = 3$, $Re = 150$, two-dimensional simulations.

that in the lock-in range, the shedding from the upstream cylinder is also synchronised with the motion of the downstream cylinder.

Figure 6 shows the flow fields at selected instants of the oscillation cycle, for $V_r = 10.0$. Like the single cylinder in the lock-in range, the force that drives the cylinder immediately after an extreme of displacement originates from the vortex being formed at the side of the cylinder closer to the wake centreline, as can be seen in figure 6(a). Also similarly to the single cylinder at synchronisation, the force that mostly contributes to the cylinder deceleration

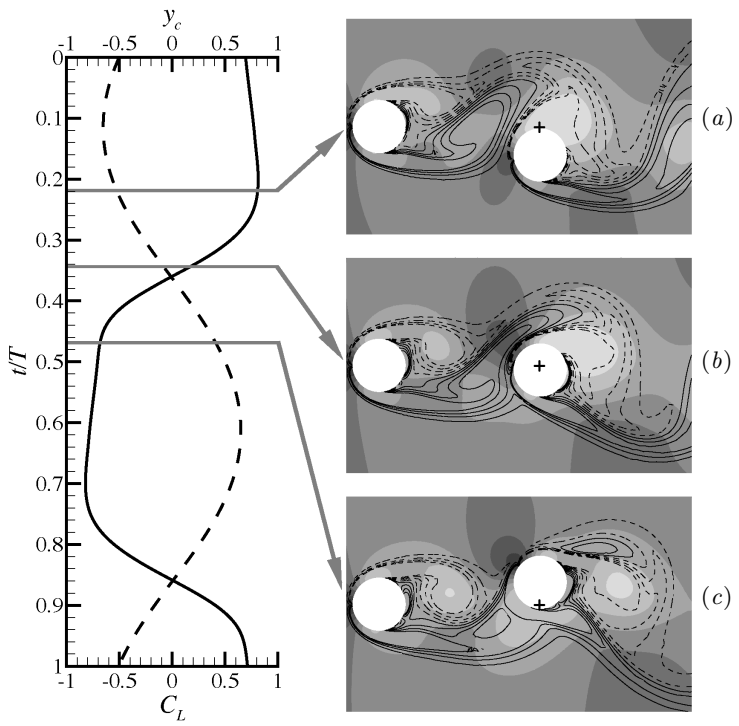

Fig. 6. *Left* – Graph of the lift coefficient (solid) and cylinder displacement (dashed) over one cycle. *Right* – vorticity iso-lines superposed on pressure contours at selected instants of the oscillation cycle. Continuous lines represent positive vorticity and dashed lines represent negative vorticity. Dark grey contours represent high pressures and light grey contours represent low pressures. The cross indicates the neutral position of the cylinder. The arrows indicate the moment of the cycle each of the flow fields refers to. Two-dimensional flow around two cylinders in tandem with $L_x/D = 3$, $V_r = 10.0$, $Re = 150$.

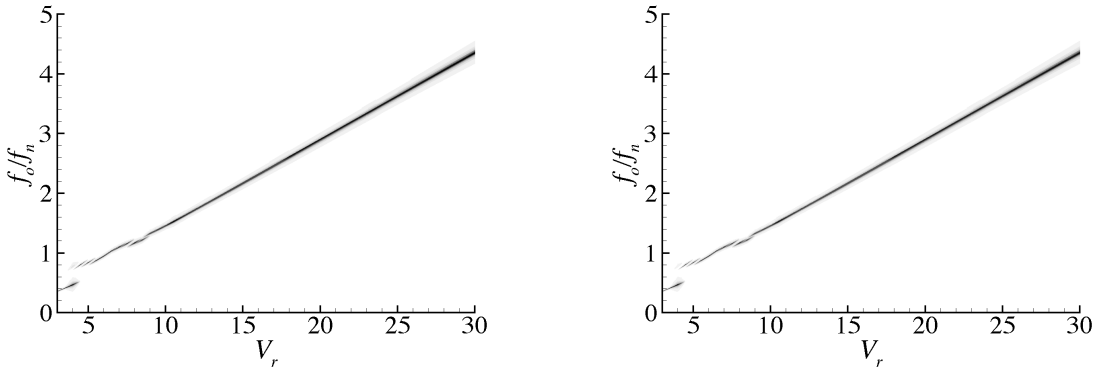

(a) Downstream cylinder y_c (b) Upstream cylinder C_L

Fig. 7. Contours of normalised power spectral density of the cylinder displacement signal, as a function of the reduced velocity. $L_x/D = 3$, $Re = 150$, two-dimensional simulations.

when the body is approaching an extreme of displacement is the high pressure of the stagnation point shifted to the outer part of the wake, as illustrated in figure 6(c). The difference is that for the tandem arrangement, the shifting of the front stagnation point does not depend exclusively on the motion of the cylinder, but is decisively influenced by the oscillatory flow upstream.

3.1.3. Tandem arrangements – large separations

For the largest separations investigated, $L_x/D = 5$ and $L_x/D = 8$, the structural response differed from what was observed for the isolated cylinder and for the tandem arrangements with smaller separations. The results for $L_x/D = 5$ and $L_x/D = 8$ exhibited the same behaviour; shown in figure 8 are the results for $L_x/D = 8$. The first difference from the smaller separations data is the presence of an easily identified lock-in region: for $5.0 \lesssim V_r \lesssim 15.0$ the cylinder vibrates at a frequency close to the structural natural frequency, instead of following the Strouhal frequency. In this range, the shedding from the downstream cylinder has a strong component at the natural frequency of the structure. It is worth highlighting that the synchronisation range is much wider for $L_x/D = 8$ and $L_x/D = 5$ than for the single cylinder case. Another evident feature of the large separation arrangements' lock-in region is a secondary peak in the amplitude, appearing where the Strouhal frequency is approximately equal to $1.5f_n$. At the higher end of the synchronisation region, the amplitude of vibration levels out smoothly to a value which is significantly higher than that observed for the single cylinder case, but lower than those observed for the small separations. This large vibration appears to be sustained indefinitely for high reduced velocities.

In figure 8 only the frequency with the highest energy is plotted. However, there are important components of the force spectrum at other frequencies. The PSD contours of the displacement signal shown in figure 9(a) reveal how the secondary peaks in the spectrum vary with the reduced velocity. The peaks at the higher frequencies, which follow a straight line of positive slope, correspond to the shedding from the upstream cylinder. This can be verified by comparing this curve with that in figure 9(b), which shows the PSD of the upstream cylinder lift coefficient signal. The peaks at the lower frequencies in figure 9(a) do not have the same origin for the entire range of reduced velocities. Within the lock-in range ($5.0 \lesssim V_r \lesssim 15.0$), these peaks are at frequencies close to the natural frequency of the structure, as expected. It is interesting to notice that the vibration of the downstream cylinder does not affect the shedding of the upstream cylinder. This is an important difference between the responses of the downstream cylinder in tandem arrangements with small and large separations, since the results for small separations in section 3.1.3. showed that in the lock-in range, the shedding from the upstream cylinder was synchronised with the downstream cylinder oscillation.

For reduced velocities higher than those of the lock-in, figure 9(a) shows that the lower frequency peaks follow another straight line of positive slope. The frequencies on this line are approximately half of the frequency of the

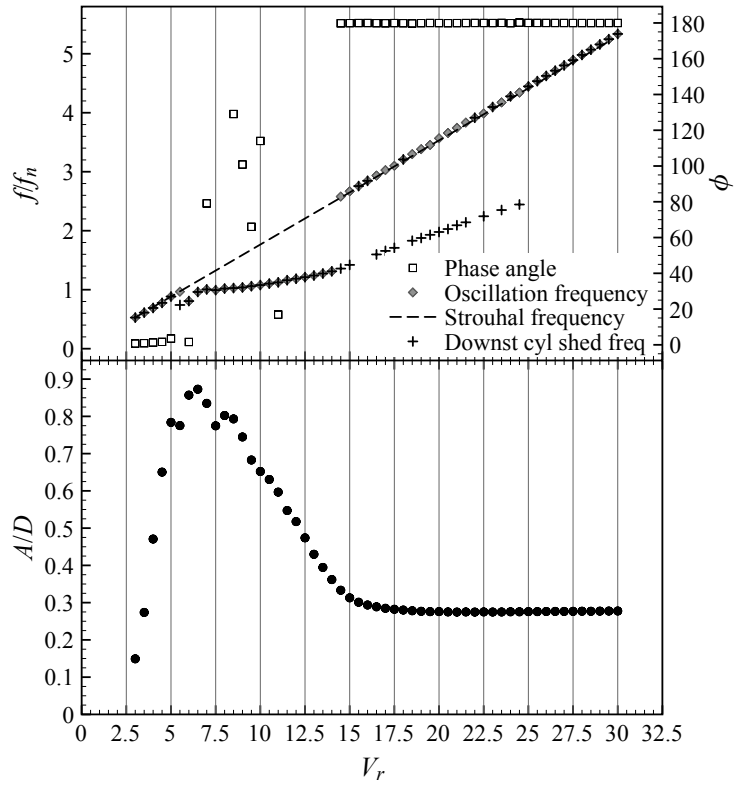

Fig. 8. Amplitude, phase angle and frequency plots against reduced velocity for the for the downstream cylinder in a tandem arrangement with $L_x/D = 8$, $Re = 150$, two-dimensional simulations.

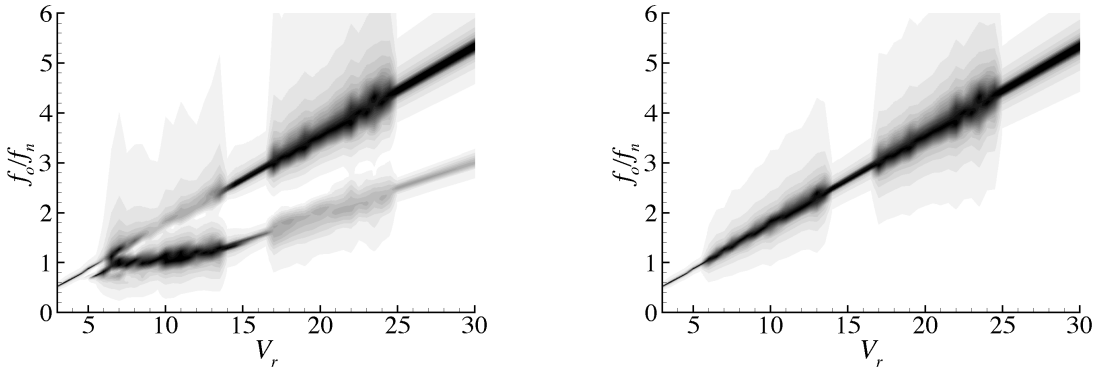

(a) Downstream cylinder y_c (b) Upstream cylinder C_L

Fig. 9. Contours of normalised power spectral density of the cylinder displacement signal, as a function of the reduced velocity. $L_x/D = 8$, $Re = 150$, two-dimensional simulations.

upstream cylinder shedding at the same reduced velocity. These peaks originate from the interaction between the vortices in the wake of the downstream cylinder, which gives rise to the secondary wake observed for tandem and staggered arrangements with streamwise separation larger than the drag inversion spacing. As reported in Carmo et al. (2008), the secondary wake has a dominant frequency equal to half the frequency of vortex shedding. It

seems that the formation of the secondary wake has a strong influence on the forces and consequently the response of the downstream cylinder, since it can delay or anticipate the shedding of the vortices. Like the arrangements with smaller separations, the two main mechanisms responsible for the excitation of the cylinder are the lower pressure regions generated by the vortices being shed and the shifting of the high pressure region at the front stagnation point.

In figure 10 it can be seen that the time histories of the lift coefficient and displacement are not regular, even at the lock-in. This reflects in the spectra shown in the same figure, which exhibit many spikes. The fact that the shedding from the upstream cylinder shows a rather clean spectrum (figure 9(b)) suggests that this irregular character of the response has its origins in the wake downstream of the leeward cylinder. The time history in figure 10(a) shows that when the reduced velocity is close to the first peak of amplitude in the synchronisation range, the phase angle jumps intermittently from a value close to 0° to a value close to 180°. When the forces are in phase with the displacement, the cylinder experiences its higher amplitudes of vibration; the shear layers separating from the leeward cylinder interact and the wake formed downstream is regular, as illustrated in figure 11(a). However, this state is not sustained when the amplitudes get too large, the phase angle shifts to a value close to 180° and the amplitude decreases gradually, until one of the vortices from the upstream cylinder impinges on the downstream cylinder at a phase which puts the force again in-phase with the displacement, and the amplitude builds-up again. This behaviour is repeated with some regularity, but is not totally periodic.

For reduced velocities close to the second peak, illustrated in figure 10(b), the phase angle varies less, with the force being out-of-phase with the displacement most of the time. The force spectra is broad-band and the amplitude of displacement shows significant modulations. Figure 11(b) shows that the shear layers in the near wake of the downstream cylinder do not interact as for the previous case ($V_r = 6.5$), and the far wake is very irregular. For higher reduced velocities (figure 10(c)), the lift coefficient and displacement time histories are considerably smoother, but the spectra show high energy at frequencies other than the Strouhal frequency, particularly at half the Strouhal frequency. This component at half the Strouhal frequency can also be identified by observing the modulation in the amplitude of displacement in the time history. The phase angle is consistently at values close to 180°, and the wake downstream is wide and irregular (figure 11(c)).

3.2. Three-dimensional simulations

A few three-dimensional simulations were performed to check the interaction between the structural response and three-dimensional structures in the flow. The Reynolds number considered was 300, which is well beyond the secondary instability in the flow around a single cylinder. The results for each configuration are presented and analysed in the following sections.

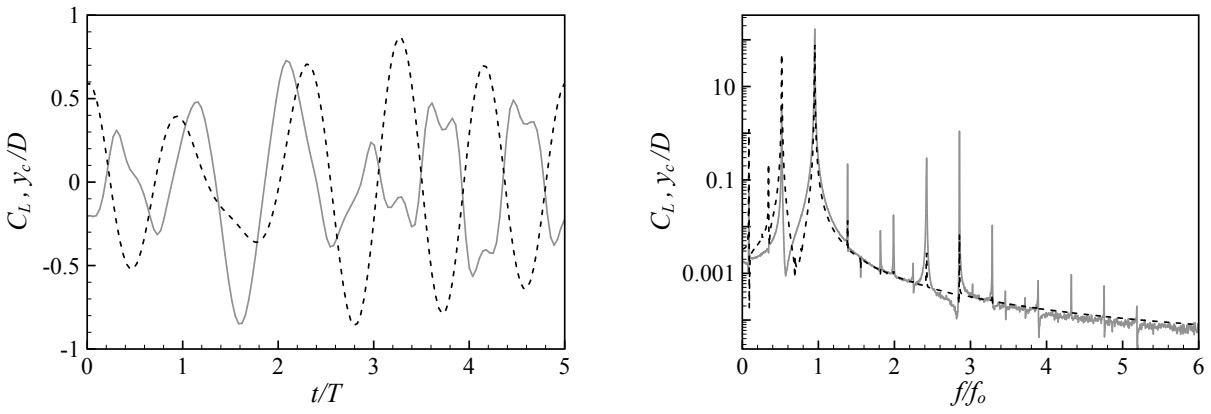

(a) $V_r = 6.5$

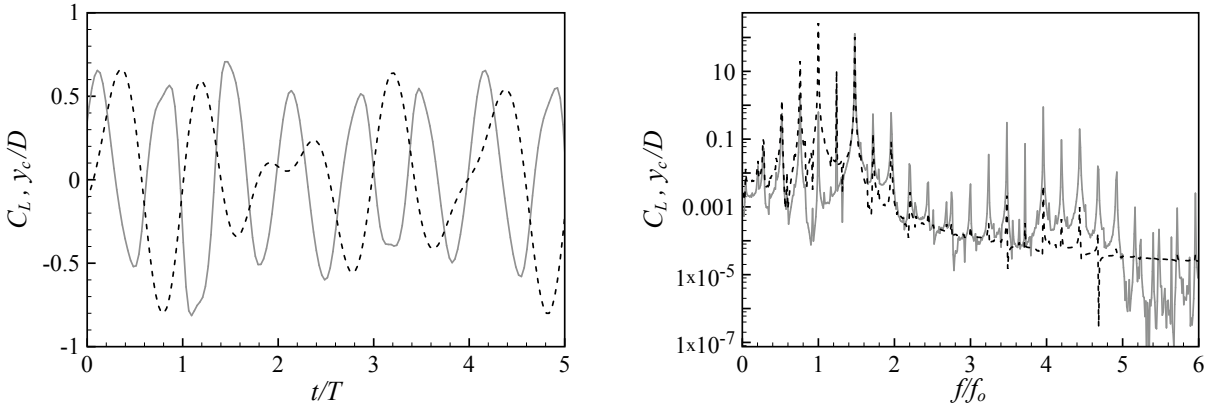

(b) $V_r = 8.5$

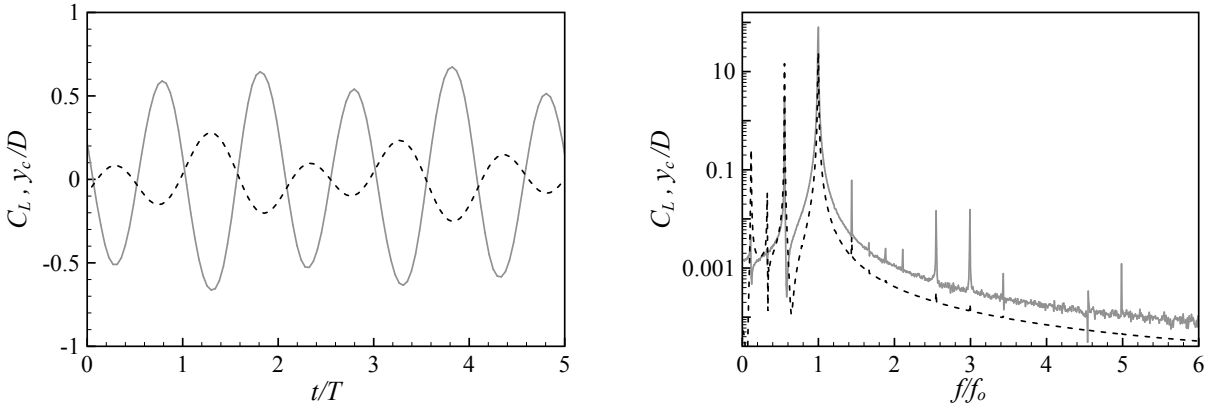

(c) $V_r = 20.0$

Fig. 10. Downstream cylinder lift coefficient (solid lines) and displacement (dashed lines) time history (left) and spectra (right). $L_x/D = 8$, $Re = 150$, two-dimensional simulations.

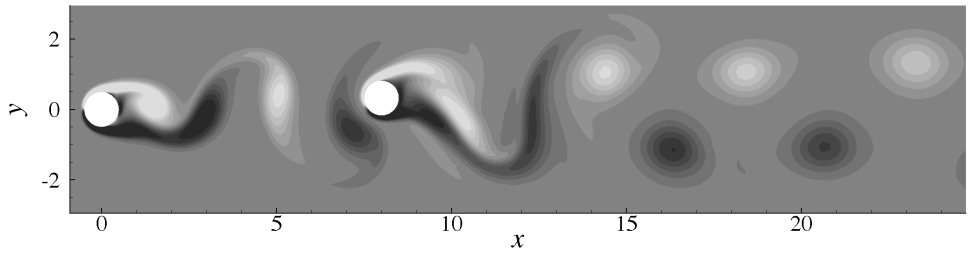

(a) $V_r = 6.5$

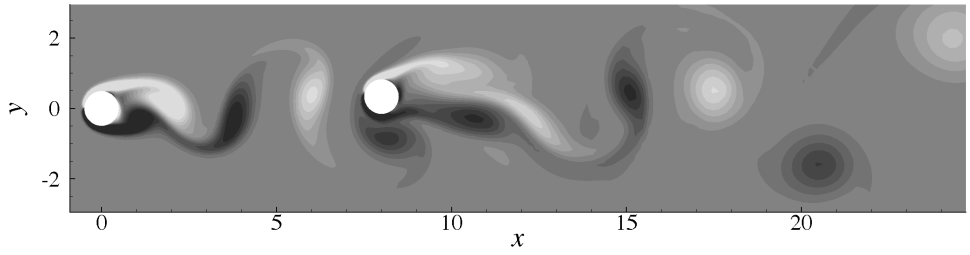

(b) $V_r = 8.5$

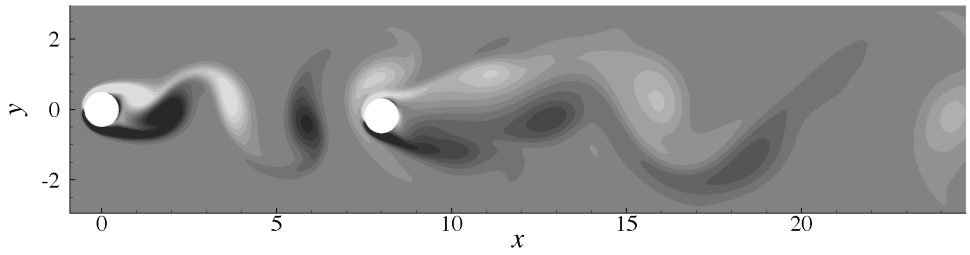

(c) $V_r = 20.0$

Fig. 11. Instantaneous vorticity contours for diverse reduced velocities, $L_x/D = 8$, $Re = 150$, two-dimensional simulations.

3.2.1. Single cylinder

Figure 12 displays the amplitude results obtained with two- ($Re = 150$) and three-dimensional ($Re = 300$) simulations. Although it was not possible to obtain enough points to draw the complete curve for the three-dimensional simulations due to the high cost of the computations, it can be seen that the three-dimensional results follow the same trend of the two-dimensional data. It seems that the Reynolds number tested is still too low to obtain an upper branch of response, observed in the experiments of Khalak and Williamson (1999).

Further insight into the three-dimensional results can be gained by studying the vorticity iso-surfaces in figure 13. For reduced velocities in the initial branch the flow is actually two-dimensional, as shown by the vorticity field illustrated in figure 13(a). It seems that the wake resulting from the vibration of the cylinder in the initial branch ($\phi \approx 0^\circ$) is stable to three-dimensional perturbations for Reynolds numbers considerably higher than the fixed cylinder critical Reynolds number. At the lower branch, three-dimensional structures do develop in

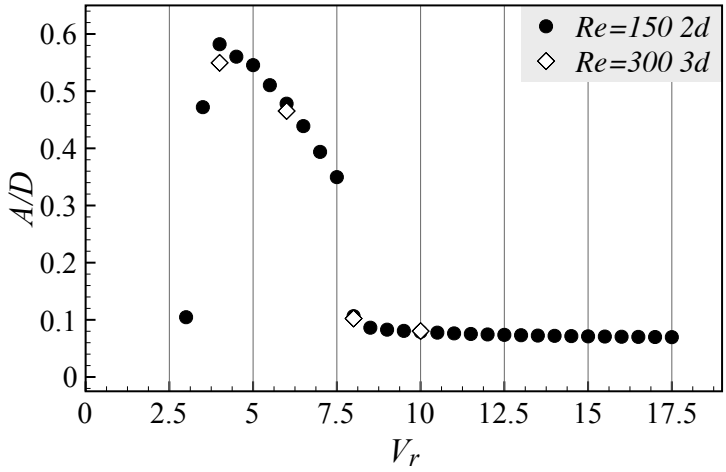

Fig. 12. Comparison between the amplitudes of vibration obtained from two- (closed symbols) and three-dimensional (open symbols) simulations, single cylinder.

the wake, as shown in figure 13(b). The streamwise vorticity contours are similar to those observed for mode B (Williamson, 1996), with streamwise vortices concentrated in the shear layer, same spatio-temporal symmetry and spanwise wavelength approximately equals to $1D$. However, the spanwise correlation of the vortex tubes is still high, as evidenced by the presence of wavy but vertical tubes far downstream. Finally, for reduced velocities higher than those of the synchronisation range, the wake also exhibits three-dimensional structures, as can be seen in figure 13(c). Once more, the streamwise vortices show strong similarity with those of mode B. Note that the spanwise correlation of the vortex tubes is notably poorer than for reduced velocities in the lower branch.

3.2.2. $L_x/D = 1.5$

The amplitude of response of the downstream cylinder in the configuration with streamwise separation $L_x/D = 1.5$ obtained from three-dimensional simulations for diverse reduced velocities is plotted in figure 14 together with the results obtained for $Re = 150$ with two-dimensional simulations. Like in the single cylinder results, the amplitudes for $Re = 300$ follow the same trend as those calculated for $Re = 150$. However, an important difference is that for $L_x/D = 1.5$, the amplitudes of the three-dimensional simulations were higher than those of the two-dimensional simulations, while the inverse occurred for the single cylinder and all the other configurations.

The vorticity iso-surfaces plotted in figure 15 help to explain this behaviour: the flow field in the proximity of the cylinders is actually two-dimensional. The fact that the flow is essentially two-dimensional for this configuration is in line with the results reported in Carmo et al. (2010), in which linear stability calculations predicted a critical Reynolds number for the onset of three-dimensional instabilities of $Re_c = 315 \pm 1$. Since the oscillation of the cylinder usually improves the spanwise correlation of the vortices, one should expect that the critical Reynolds number of the arrangement with an elastically-mounted downstream cylinder would be equal or higher than that

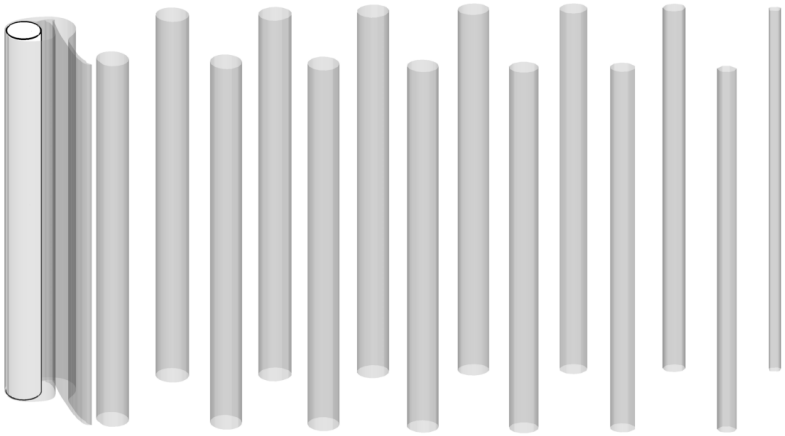

(a) $V_r = 4.0$

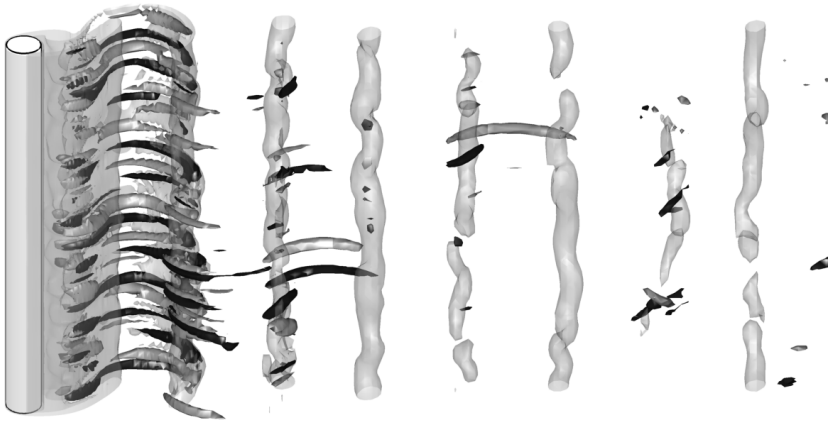

(b) $V_r = 6.0$

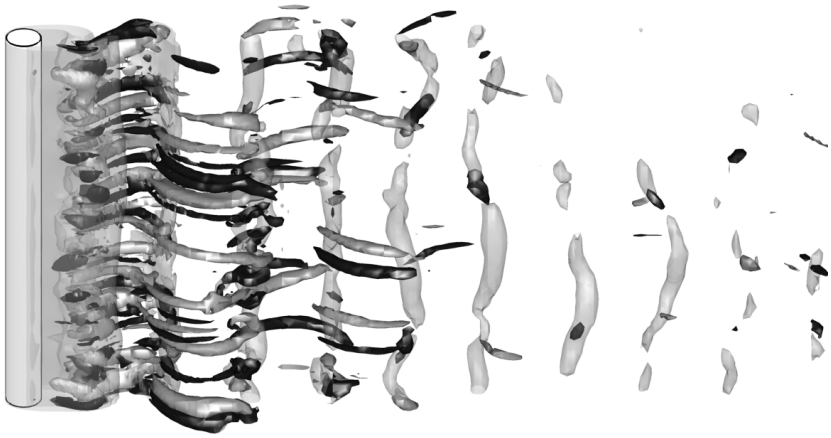

(c) $V_r = 8.0$

Fig. 13. Instantaneous iso-surfaces of spanwise vorticity (translucent surfaces) and streamwise vorticity (solid surfaces) for diverse reduced velocities. Solid light grey and dark grey surfaces represent iso-surfaces of negative and positive ω_x respectively. Single cylinder, $Re = 300$, three-dimensional simulations.

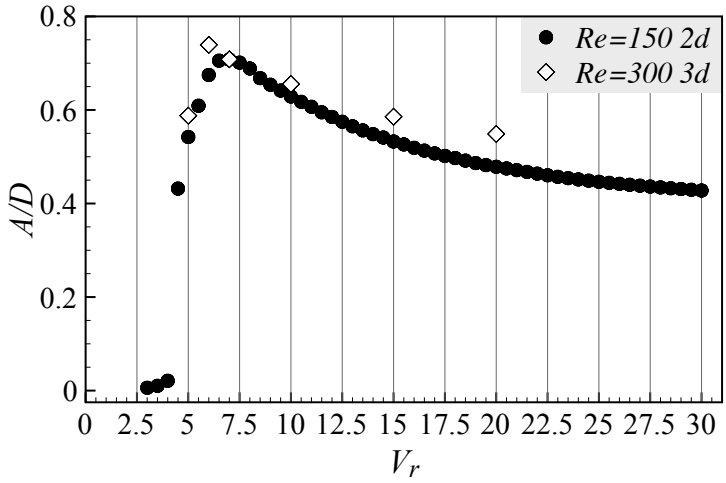

Fig. 14. Comparison between the amplitudes of vibration obtained from two- (closed symbols) and three-dimensional (open symbols) simulations, $L_x/D = 1.5$.

of the arrangement with fixed cylinders.

Curiously, for reduced velocities in the lower branch, three-dimensional structures develop far downstream, as illustrated in figure 15(b). However, the influence of these flow structures on the forces applied on the cylinder is negligible, and the spanwise correlation of the lift and drag is perfect. Three-dimensional structures in the far wake were also observed in the numerical simulations reported by Carmo and Meneghini (2006), and in that case these structures were also observed to have no effect in the forces imposed on the cylinder. It seems that such structures arise from convective instabilities in the far wake; this could explain why they were not captured in the linear stability analysis described in Carmo et al. (2010), since that kind of analysis only captures absolute asymptotic instabilities.

3.2.3. $L_x/D = 3$

The amplitude results shown in figure 16 show that also for $L_x/D = 3$ the results for $Re = 300$ follow the trend observed for $Re = 150$. The main difference between these results and those obtained for $L_x/D = 1.5$ shown in figure 14 is that for $L_x/D = 3$ the amplitudes obtained for $Re = 300$ are slightly smaller. This is because the flow field is strongly three-dimensional, as further investigation reveals.

At the initial branch (figure 17(a)), the effect of the three-dimensional instabilities is so strong that the spanwise vortices completely disappear a few diameters downstream of the arrangement. It can be seen that the streamwise vortices develop close to the wall of the downstream cylinder; this fact added to the strong coupling between the spanwise vortices and three-dimensional instabilities indicate that the dominant mode in such flows must be mode T3 (Carmo et al., 2010).

The three-dimensional structures are completely different at the lower branch. Figure 17(b) shows that at

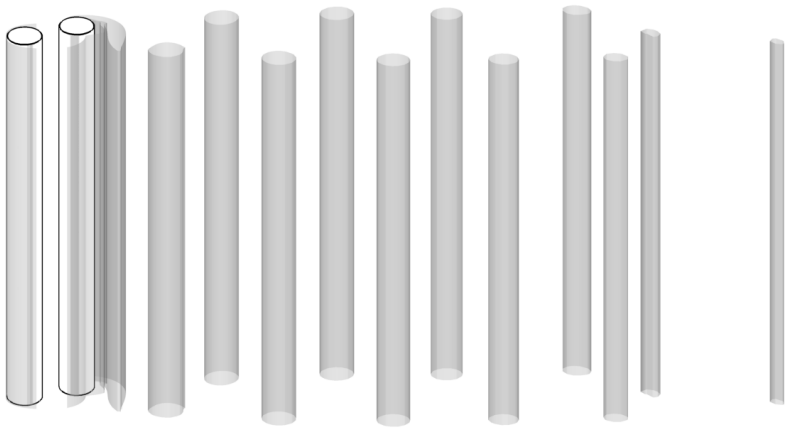

(a) $V_r = 5.0$

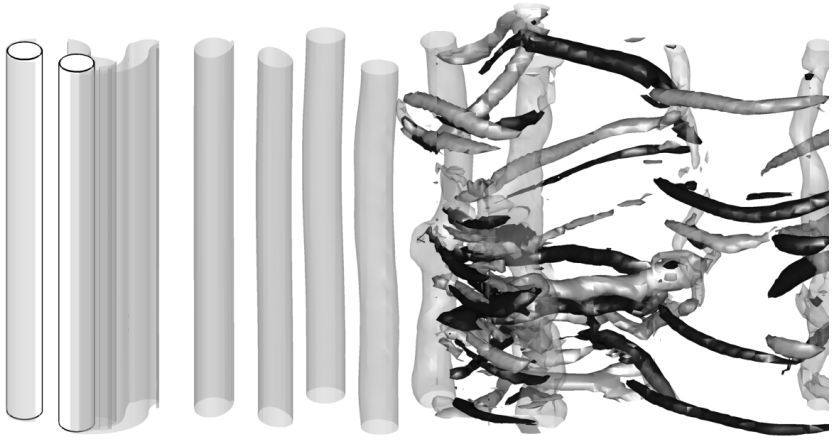

(b) $V_r = 7.0$

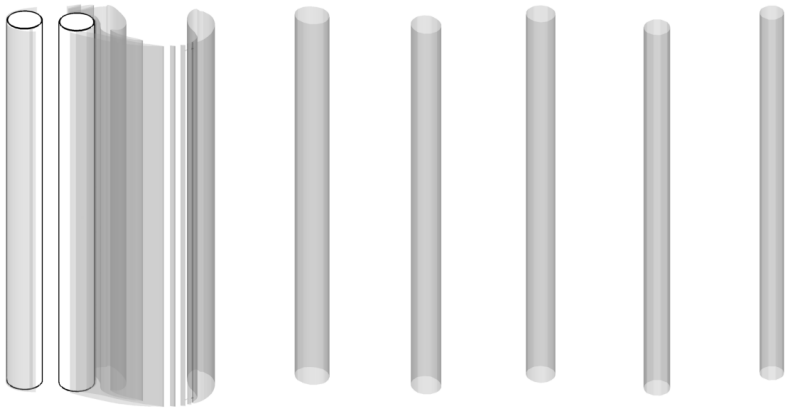

(c) $V_r = 15.0$

Fig. 15. Instantaneous iso-surfaces of spanwise and streamwise vorticity for diverse reduced velocities, $L_x/D = 1.5$, $Re = 300$, three-dimensional simulations. Surfaces are as in figure 13.

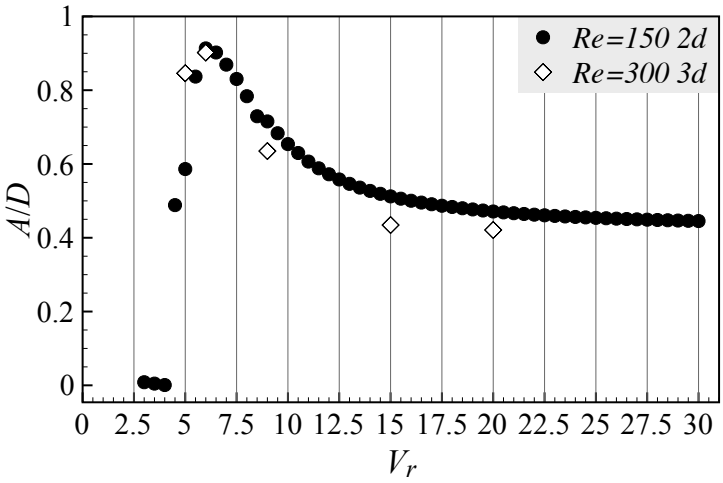

Fig. 16. Comparison between the amplitudes of vibration obtained from two- (closed symbols) and three-dimensional (open symbols) simulations, $L_x/D = 3$.

$V_r = 6.0$ the streamwise vortices originate in the base region of the upstream cylinder and are similar to those characteristic of mode B. The spanwise vortices persist until far downstream, although they show considerable waviness. It is remarkable that flows in the initial and lower branches, which have very similar reduced velocities and amplitude of response, can be so fundamentally different.

For reduced velocities high enough to be outside the synchronisation range, strong streamwise vorticity is still observed, as can be seen in figure 17(c). However, these three-dimensional structures are clearly less persistent than for the reduced velocities in the lower branch (figure 17(b)), and also have a larger spanwise wavelength. The spanwise vortices still show high spanwise correlation, probably due to the high amplitude of vibration of the downstream cylinder.

3.2.4. $L_x/D = 5$ and $L_x/D = 8$

The results of the simulations of the FIV at $Re = 300$ for the configurations with larger separations, $L_x/D = 5$ and $L_x/D = 8$, also showed the same trend as the results obtained for $Re = 150$, as can be seen in figure 18. There is a well-defined lock-in region, followed by a plateau at higher reduced velocities. In general, the amplitude of response at $Re = 300$ was slightly lower than those at $Re = 150$ at the same reduced velocities. This is because the presence of three-dimensional structures increases the transport of vorticity from the main spanwise cores and de-correlates the forces in the spanwise direction. These phenomena make the resulting forces on the downstream cylinder less intense, counter-balancing the effect of the increase of the Reynolds number.

Figure 19 shows iso-surfaces of spanwise and streamwise vorticity for selected reduced velocities. It can be seen that the flow is indeed strongly three-dimensional for all the range of reduced velocities. The streamwise vortices develop in the near wake of the upstream cylinder, and have predominantly the characteristics of mode B.

(a) $V_r = 5.0$

(b) $V_r = 6.0$

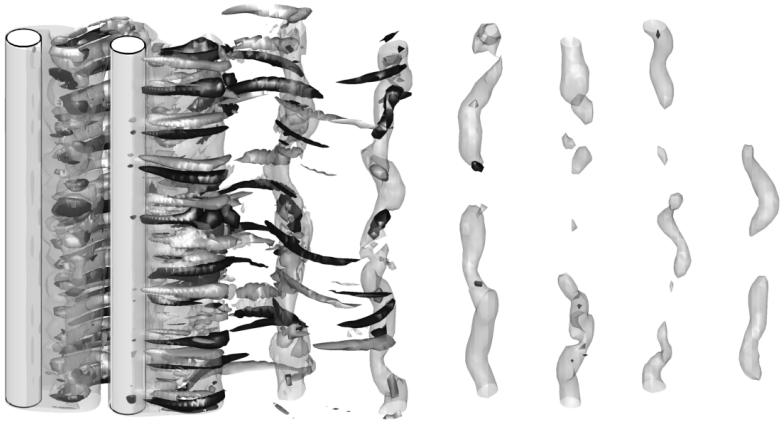

(c) $V_r = 15.0$

Fig. 17. Instantaneous iso-surfaces of spanwise and streamwise vorticity for diverse reduced velocities, $L_x/D = 3$, $Re = 300$, three-dimensional simulations. Surfaces are as in figure 13.

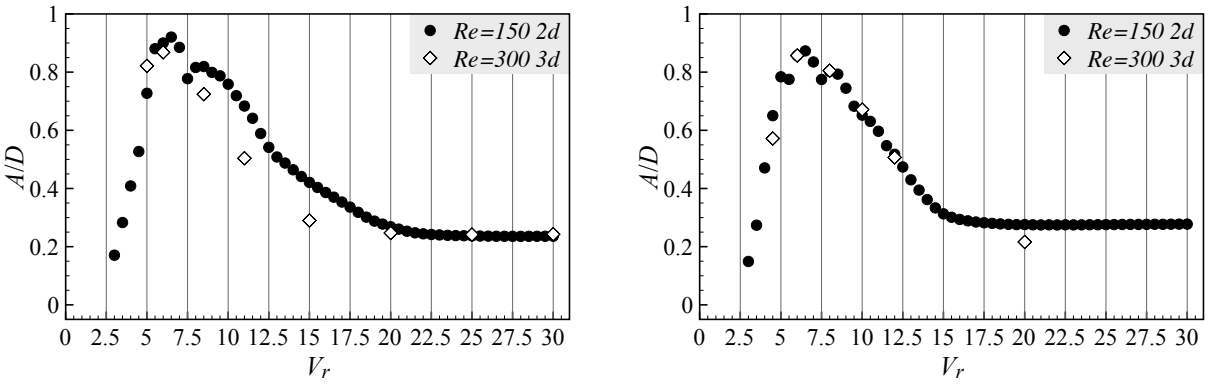

(a) $L_x/D = 5$ (b) $L_x/D = 8$

Fig. 18. Comparison between the amplitudes of vibration obtained from two- (closed symbols) and three-dimensional (open symbols) simulations, $L_x/D = 5$ and $L_x/D = 8$.

The braids of streamwise vortices break down when they approach the downstream cylinder, and no organised streamwise vorticity pattern can be observed further downstream. This is consistent with the results obtained in the investigation of the secondary instabilities in the wake of fixed arrangements performed by Carmo et al. (2010). It seems that, for separations larger than the drag inversion spacing, the motion of the downstream cylinder does not change the sensitivity of the flow to three-dimensional perturbations and the evolution of the three-dimensional structures as they are convected.

4. Discussion

4.1. *Two-dimensional* vs *three-dimensional simulations*

When performing numerical simulations of flows it is worth investigating whether two-dimensional calculations are enough to capture the relevant physical mechanisms or it is necessary to resort to expensive three-dimensional calculations. This is particularly relevant in parametrical studies, as the number of cases to be simulated are usually large. The results presented in this paper may provide some guidance regarding this question for future studies.

For all the configurations investigated, the three-dimensional results were observed to follow the same trend as the two-dimensional results. However, the flow field is strongly three-dimensional for most of the configurations, and it is likely to be like that for all configurations if the Reynolds number is further increased. Obviously, this makes the quantitative match between two-dimensional and three-dimensional results, or two-dimensional and experimental results, seem improbable. So if one is interested in obtaining accurate values of the forces or structural response, there is no doubt that three-dimensional calculations are strictly necessary.

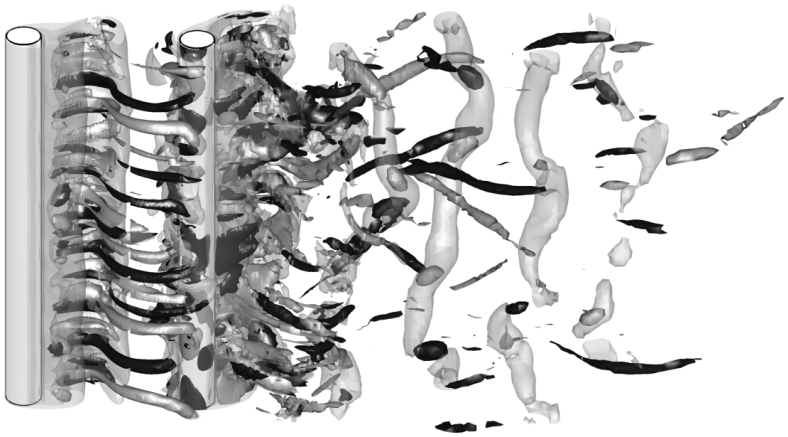

(a) $L_x/D = 5$, $V_r = 6.0$

(b) $L_x/D = 5$, $V_r = 8.5$

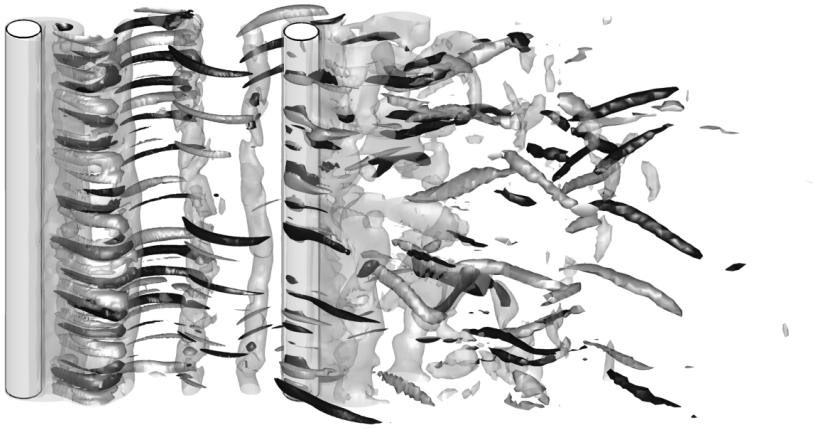

(c) $L_x/D = 8$, $V_r = 20.0$

Fig. 19. Instantaneous iso-surfaces of spanwise and streamwise vorticity for diverse reduced velocities, $L_x/D = 5$ and $L_x/D = 8$, $Re = 300$, three-dimensional simulations. Surfaces are as in figure 13.

However, we have to consider that the high cost of ALE simulations per se added to the cost of running the calculations in three-dimensions makes a rigourous parametric study incredibly challenging. It seems that given the computational power currently available, a better strategy would be to sweep the parameter space with two-dimensional calculations, and then use three-dimensional simulations to study in depth the cases of interest, or representative cases of the different behaviours observed. Needless to say, this approach is valid only when the relevant physical features of the phenomenon are essentially two-dimensional and properly captured by the two-dimensional simulations. The results presented in this paper showed that this is the case for the FIV of the downstream cylinder in the flow around circular cylinders in tandem for moderate Reynolds numbers ($Re \leq 500$). For higher Reynolds numbers, it should be remembered that an upper branch of response is observed in the VIV of an isolated cylinder (Khalak and Williamson, 1999). It is possible that the response of a downstream cylinder in a tandem arrangement is not affected in the same way, so this Reynolds number limit could be increased. In fact, the experimental results of FIV of cylinders in tandem arrangements at higher Reynolds numbers available in the literature do not show the presence of an upper branch in the response of the downstream cylinder (Bokaian and Geoola, 1984; Zdravkovich, 1985; Brika and Laneville, 1999; Hover and Triantafyllou, 2001). Nonetheless, further investigations are necessary in order to assure that three-dimensional structures do not change fundamental characteristics of the flow at higher Reynolds numbers.

4.2. Physical mechanism

We have seen that the forces applied on the downstream cylinder have two main origins: the vortices shed from the downstream cylinder, which produce low pressure regions in the vicinity of the body; and the shifting of the front stagnation point, which is an area of high pressure. In the flow around a single cylinder, the low pressure regions generated by the vortices shed are also present, so the shifting of the front stagnation point must be the main reason for the differences observed between the responses of an isolated cylinder and of the downstream cylinder in tandem arrangements, both at the lock-in and at higher reduced velocities.

In the flow around tandem arrangements, the position of the stagnation point oscillates along the front portion of the surface of the cylinder because the flow in the gap between the bodies is oscillatory. These oscillations are more regular for configurations with small separations because the shedding of the upstream cylinder is coupled with the motion of the downstream cylinder. This kind of 'feedback' adds to the self-governing character of the vibrations, resulting in higher amplitudes of vibrations. For large separations, the shedding from the upstream cylinder does not lock to the motion of the downstream cylinder, so the oscillatory flow in the gap has a constant frequency, which is approximately equal to the shedding frequency observed for fixed arrangements. The irregularity in the motion of the downstream cylinder in such configurations is basically due to the vortex interactions downstream and also to the strong three-dimensional character of the flow in the gap.

In the framework of the equation (3), we could say that, for an isolated cylinder, the lift force depends only on $\ddot{y}_c^*$, $\dot{y}_c^*$ and t^*; it does not matter where the cylinder is located in the fluid stream. For the downstream cylinder in tandem arrangements, the lift force also depends on y_c^*, since the oscillatory flow is restricted to the wake of the upstream cylinder, and the response of the cylinder changes if its neutral position is displaced.

A natural question to be asked is whether this physical mechanism would also be able to explain the vibrations of cylinders allowed to move in the streamwise direction too or the response of configurations in which the upstream cylinder is also elastically-mounted. We argue that in such cases, the upstream cylinder would still shed vortices, so the flow in the gap would still be oscillatory. Therefore, the mechanism proposed should also be present in such cases. However, if the upstream cylinder is allowed to vibrate, the wake in the gap can be considerably different from the cases we have investigated in this paper, and this can dramatically change the response of the downstream cylinder. Particularly for small separations, the "fluid coupling" between the two cylinders is very strong, and it would not be surprising if completely unusual response characteristics were observed for each of the cylinders, specially in the synchronisation range.

Another issue worth discussing is the effectiveness of traditional FIV suppression devices, like strakes, in the tandem arrangements we have investigated. Probably the most natural decision one would make is to use these devices on the downstream cylinder only. However, it is unlikely that this approach would decrease the vibrations to a satisfactory level. These devices are primarily designed to be used on isolated cylinders, so ultimately they inhibit the vibrations by modifying or stopping the vortex shedding. However, besides the vortex shedding, the oscillatory flow in the gap is also responsible for the vibrations of the downstream cylinder in tandem arrangements. So, a completely efficient solution would also have to act on the flow in the gap, and this almost certainly means that some sort of modification must be carried out on the upstream cylinder too, so as to prevent the vortex shedding from this body.

4.3. Comparison with experimental data

According to the previously published experimental research (Bokaian and Geoola, 1984; Hover and Triantafyllou, 2001; Assi et al., 2008), the downstream cylinder in tandem arrangements experiences amplitudes of vibration higher than those experienced by an isolated cylinder in the lock-in, and when the mass ratio is sufficiently low, the amplitudes of vibration are also significant for higher reduced velocities. The computational results presented in this paper were able to reproduce high amplitude vibrations both in the lock-in and for higher reduced velocities. However, an important difference between our results and previously published experimental data is that, for reduced velocities higher than those of the lock-in range, the amplitude of vibration of the downstream cylinder in experiments is observed to increase with reduced velocity, while in our computational results (both two- and three-dimensional) the amplitude reaches a plateau which seems to be maintained for indefinitely high reduced

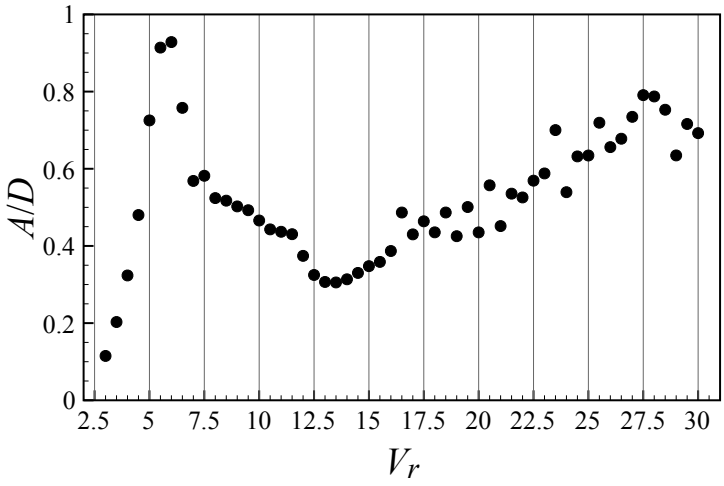

Fig. 20. Response of the downstream cylinder in a tandem arrangement with $L_x/D = 4$ with the upstream cylinder fixed, obtained with two-dimensional simulations. The reduced velocity was varied by changing the free stream speed, so $Re/V_r = 30$. The structural parameters were $m^* = 2.0$ and $\zeta = 0.0$.

velocities.

To explain the reasons for this discrepancy, it is necessary to check how exactly the phenomenon is usually investigated in computations and experiments. One of the fundamental differences between these two approaches is on the way the reduced velocity was varied. In the majority of the experimental studies, the stiffness of the structure was kept constant and the speed of the flow was varied, thus the Reynolds number varies at the same rate as the reduced velocity. In our computational simulations, the parameter that was varied was the structural stiffness, so the Reynolds number was kept constant while the reduced velocity was changed. This indicates that the Reynolds number may be fundamental in the determination of the response amplitude of the cylinder.

Figure 20 shows data from preliminary two-dimensional simulations of the FIV of the downstream cylinder in a tandem arrangement with $L_x/D = 4$, varying the reduced velocity by changing the free stream speed, so the Reynolds number varies as well. The structural parameters were $m^* = 2$ and $\zeta = 0.0$ and the ratio between Reynolds number and reduced velocity $Re/V_r = 30$. Although two-dimensional simulations are evidently not appropriate for obtaining quantitatively accurate results in flows at such Reynolds numbers, we believe they can capture the essence of the relevant physical mechanisms and provide a qualitative estimation of the actual response (see discussion in section 4.1.). It can be seen that by varying the Reynolds number with the reduced velocity the increasing trend in the amplitude is recovered, and the behaviour of the structure qualitatively matches the experimental data (see Assi et al., 2008). The data in figure 20 is part of an ongoing work which comprises a combination of experimental and computational efforts in order to achieve a deeper understanding of the mechanisms of the FIV at high reduced velocities for configurations with separations larger than the drag inversion spacing, for a large range of Reynolds numbers.

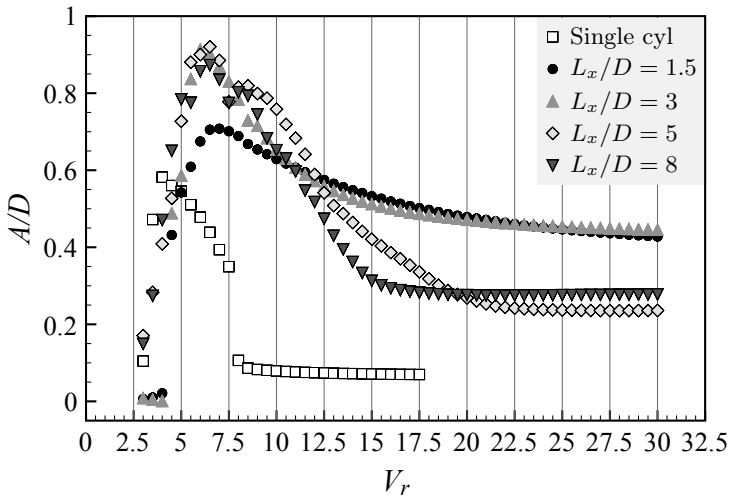

Fig. 21. Amplitude as a function of reduced velocity for all configurations. $Re = 150$, two-dimensional simulations.

5. Conclusions

We have employed direct numerical simulations to analyse the structural response and flow fields obtained for tandem arrangements with diverse centre-to-centre separations, the upstream cylinder being fixed and the downstream cylinder being free to oscillate in the transverse direction. The Reynolds numbers tested were $Re = 150$ for two-dimensional simulations and $Re = 300$ for three-dimensional simulations, and they were kept constant while the reduced velocity was varied by changing the structural stiffness.

The results showed that there are significant changes in the structural response of the downstream cylinder in the tandem arrangements when compared to an elastically mounted single cylinder. The amplitude results of the two-dimensional simulations are plotted together in figure 21. In this figure, it can be seen that the lock-in region boundaries are modified: it is difficult to define an upper limit for configurations with small separations ($L_x/D \leq 3$) and for larger cylinder separations, the lock-in region is much wider than in the single cylinder case. The maximum displacement amplitude observed in the synchronisation range is also larger, approaching values 50% higher than the maximum displacement amplitude of the single cylinder case. In addition, the displacement amplitude responses at high reduced velocities were very significant, in some cases comparable to the highest amplitude in the single cylinder case. The physical mechanism responsible for these differences appears to be related to the oscillatory flow in the gap between the cylinders, which causes the front stagnation point of the downstream cylinder to shift alternatively along the upstream portion of the cylinder wall.

The three-dimensional simulations highlighted that, for fixed Reynolds number simulations within the Reynolds number range considered in this paper, the dynamics of the structural response were not fundamentally affected by the presence of the three-dimensional wake structures. This suggests that two-dimensional simulations may provide

some physical insights in preliminary studies at other Reynolds numbers, although they will certainly not be able to provide accurate quantitative results. Also, it was noticed that the vibration of the cylinder improves the spanwise correlation of the vortices, although it is not generally sufficient to make the flow completely two-dimensional. Interestingly, some of the three-dimensional instabilities investigated in the flow around fixed cylinders were also observed in the three-dimensional FIV simulations. The presence of three-dimensional structures in the flow causes the spectra of displacement and force to be broad-band.

Although many insights were gained from the FIV results reported in this paper, there is still a number of issues that remain to be investigated. One of them is the dependence of the response on the Reynolds number, and this question is already being addressed by the authors. Other topics that are worth investigating are the FIV of cylinders allowed to move in the streamwise as well as the cross-stream direction, the FIV in arrangements where the upstream cylinder is also compliantly-mounted, the development of reduced models to predict the response of the cylinders and the design of effective FIV suppressors for flows with wake interference.

Acknowledgement

The authors would like to thank Gustavo Assi for the enlightening discussions about this work. B.S.C. acknowledges the support from Capes / MEC - Brazil during his PhD at Imperial College London.

References

Assi, G. R. S., Bearman, P. W., Meneghini, J. R., 2008. Unsteady response of a circular cylinder under wake-induced excitation from a fixed upstream cylinder. In: Zoloratev, I., Horáček, J. (Eds.), Flow-Induced Vibration 2008. Prague, Czech Republic.

Assi, G. R. S., Meneghini, J. R., Aranha, J. A. P., Bearman, P. W., Casaprima, E., 2006. Experimental investigation of flow-induced vibration interference between two circular cylinders. Journal of Fluids and Structures 22, 819–827.

Batina, J. T., August 1990. Unsteady euler airfoil solutions using unstructured dynamic meshes. AIAA Journal 28 (8), 1381–1388.

Beskok, A., Warburton, T. C., 2001. An unstructured hp finite-element scheme for fluid flow and heat transfer in moving domains. Journal of Computational Physics 174, 492–509.

Bokaian, A., Geoola, F., 1984. Wake-induced galloping of two interfering circular cylinders. Journal of Fluid Mechanics 146, 383–415.

Brika, D., Laneville, A., 1999. The flow interaction between a stationary cylinder and a downstream flexible cylinder. Journal of Fluids and Structures 13, 579–606.

Carmo, B. S., 2005. Numerical investigation of the flow around two cylinders in tandem arrangements. MSc dissertation, Escola Politécnica - University of São Paulo, Brazil.

Carmo, B. S., 2009. On wake interference in the flow around two circular cylinders: direct stability analysis and flow-induced vibrations. Ph.D. thesis, Imperial College London.

Carmo, B. S., Meneghini, J. R., 2006. Numerical investigation of the flow around two circular cylinders in tandem. Journal of Fluids and Structures 22, 979–988.

Carmo, B. S., Meneghini, J. R., Sherwin, S. J., 2010. Secondary instabilities in the flow around two circular cylinders in tandem. Journal of Fluid Mechanics 644, 395–431.

Carmo, B. S., Sherwin, S. J., Bearman, P., Willden, R., 2008. Wake transition in the flow around two circular cylinders in staggered arrangements. Journal of Fluid Mechanics 597, 1–29.

Hover, F. S., Triantafyllou, M. S., 2001. Galloping response of a cylinder with upstream wake interference. Journal of Fluids and Structures 15, 503–512.

Jester, W., Kallinderis, Y., 2004. Numerical study of incompressible flow about transversely oscillating cylinder pairs. Journal of Offshore Mechanics and Arctic Engineering - Transactions of the ASME 126, 310–317.

Karniadakis, G. E., Israeli, M., Orszag, S. A., 1991. High-order splitting methods for the incompressible Navier–Stokes equations. Journal of Computational Physics 97, 414–443.

Karniadakis, G. E., Sherwin, S. J., 2005. Spectral/hp Element Methods for Computational Fluid Dynamics, 2nd Edition. Oxford University Press, Oxford-UK.

Khalak, A., Williamson, C. H. K., 1999. Motions, forces and mode transitions in vortex-induced vibrations at low mass-damping. Journal of Fluids and Structures 13 (7-8), 813–851.

King, R., Johns, D. J., 1976. Wake interaction experiments with two flexible circular cylinders in flowing water. Journal of Sound and Vibration 45 (2), 259–283.

Li, L., Sherwin, S. J., Bearman, P. W., 2002. A moving frame of reference algorithm for fluid/structure interaction of rotating and translating bodies. International Journal for Numerical Methods in Fluids 38, 187–206.

Mittal, S., Kumar, V., 2001. Flow-induced oscillations of two cylinders in tandem and staggered arrangements. Journal of Fluids and Structures 15, 717–736.

Newmark, N. M., 1959. A method of computation for structural dynamics. Journal of the Engineering Mechanics Division of ASCE 85, 67–94.

Papaioannou, G. V., Yue, D. K. P., Triantafyllou, M. S., Karniadakis, G. E., AUG 2008. On the effect of spacing on the vortex-induced vibrations of two tandem cylinders. Journal of Fluids and Structures 24 (6), 833–854.

Williamson, C. H. K., 1996. Three-dimensional wake transition. Journal of Fluid Mechanics 328, 345–407.

Williamson, C. H. K., Govardhan, R., 2004. Vortex-induced vibrations. Annual Review of Fluid Mechanics 36 (413-455).

Zdravkovich, M. M., 1985. Flow-induced oscillations of two interfering circular cylinders. Journal of Sound and Vibration 101 (4), 511–521.

Zdravkovich, M. M., 1987. The effects of interference between circular cylinders in cross flow. Journal of Fluids and Structures 1 (2), 239–261.